Transactions of the Materials Research Society of Japan 29 [8] 3533-3538 (2004)

Characteristic Microstructure Features Influencing the Mechanical Behavior of the Warm-Rolled Ultrafine Low-Carbon Steel

Fuxing Yin, Toshihiro Hanamura, Tadanobu Inoue and Kotobu Nagai
Steel Research Center, National Institute of Materials Science,
Tsukuba, 305-0047, JAPAN
Fax: 81-29-859-2101, e-mail: YIN.Fuxing@nims.go.jp

The microstructural feature of the warm-rolled ultrafine low-carbon steel was examined with orientation imaging microscopy (OIM) and TEM. Biaxial warm-rolling caused the elongated ferrite grains together with the preferred grain orientations, and the high density of retained dislocations in the ultrafine-grained microstructure. Based on the cell-block boundary (CBB) model proposed by Peeters, the critical resolved shear stress (CRSS) on 112 and 110 slip systems was calculated, by distinguishing the anisotropy effects of CBBs on the two slip systems. It was observed that the CRSS ratio on 112 and 110 slip systems was 0.99 in both the as-rolled and annealed conditions. With the CRSS ratio Taylor factor that was used to predict the strength contributions of the microstructure features was obtained. The contributions of solid solution, grain refinement, cementite particle dispersion, and dislocations to the mechanical behavior of the ultrafine-grained low-carbon steels were estimated and a good agreement was reached between the estimation and experimental results of yield strength.
Key words: Electron backscattering diffraction (EBSD), Low-carbon steel, Texture, Critical resolved shear stress, Dislocation

1. INTRODUCTION

The yield strength of low-carbon ferrite-pearlite steels can be approximately estimated by a linear sum of the solid solution effect, grain refinement effect, and the effects of pearlite fraction. Compared with the equiaxial and randomly oriented ferrite-pearlite microstructure in the normalization heat-treated low-carbon steels, the warm-rolled ultrafine-grained steels exhibit the specific microstructural features; column-shaped ferrite grains elongating along the rolling direction, preferred grain orientations, and a high density of retained dislocations [1]. Taylor factor is the unique parameter that relates the macroscopic deformation behavior of materials to the texture of the aggregated grains and the activation tolerance of the specific slip systems [2, 3]. For polycrystalline materials, Taylor averaged the factors over all the orientations and related the yield stress σ_y of polycrystals in tension to the glide yield stress τ_c by

$$\overline{M} = \sigma_y / \tau_c = < \sum_s d\gamma_s > / d\varepsilon \qquad (1)$$

The bracket in Eq. (1) indicates an average of the internal dissipation increment over all the grains in the aggregates. In BCC metals where more than one equivalent slip systems are activated during straining, $\tau_c = \tau_c^s$ relation may become invalid. In an Fe-Si alloy the CRSS of the {110}, {112} and {123} slip systems was found to be different, therefore the Taylor factor M depended upon the choice of slip systems and ξ (where ξ =CRSS$_{\{hkl\}}$/CRSS$_{\{110\}}$) [4]. Since a high density of dislocations remained in the warm-rolled low-carbon steel, a correct calculation of the Taylor factor for the textured ultrafine-grained microstructure requires the evaluation of a dislocation structure that may cause the difference of CRSS between {110} and {112} slip systems.

Peeters *et al.* idealized the dislocation patterns in deformed metals in terms of the cell-block boundaries (CBBs), irregularly oriented dislocation cell boundaries (CBs) and statistically stored dislocations according to the TEM observation [5-7]. The authors attributed the substructural anisotropy to the existence of CBBs (also called planar dislocation sheets or microbands). The CBBs developed parallel to the active slip systems, and produced the extra sliding resistances that differed on the slip systems. Hence, the CRSS of a slip system s, τ_c^s is composed of the following contributing factors;

$$\tau_c^s = \tau_0 + (1-f)\alpha G b\sqrt{\rho^{CB}} + f\sum_i \tau_{is}^{CBB} \qquad (2)$$

where τ_0 represents the initial shearing resistance of the slip system, including the intrinsic Peierls-Naborro stress and the hardening contributions except for the dislocations. Dislocations on cell boundaries with a density of ρ^{CB} are responsible for most of the isotropic hardening. α, G, and b represent the dislocation interaction parameter, the shear modulus and the magnitude of the Burgers vector, respectively. f is the

volume fraction of CBBs, and $\sum_t \tau_{is}^{CBB}$ shows the total contributions of the families of CBBs on the sliding resistance of slip system *s*.

The microstructural features, such as the dislocation density or the volume fraction of the CBBs, were obtained through calibrating the simulation model to the stress-strain response in different mechanical tests [5]. A direct characterization of the microstructural features in the ultrafine-grained steels becomes mandatory for microstructural evaluation and the prediction of mechanical anisotropic behavior. Fortunately, the advancement of the EBSD (Electron BackScattering Diffraction) technique has prompted a faster and statistically meaningful method for substructural characterization with a high spatial resolution. In the present work, EBSD and TEM investigations are carried out to characterize the substructural features in the warm-rolled ultrafine-grained steels. Since the features of the CBBs are emphasized when the plastic anisotropy of the deformed microstructure are considered, the as-rolled samples are then annealed at a temperature where only the recovery of dislocations is possible.

2. EXPERIMENTAL PROCEDURE

A low-carbon steel with the composition of 0.148C-0.33Si-1.41Mn (wt.%) was prepared by induction melting in an argon atmosphere. Steel blocks with a section of 30×30mm^2 cut from the hot-rolled steel were reheated to 1173K and quenched in water. Caliber-rolling of the steel rods was carried out while holding the rods at 923±30K. Finally, steel bars with the 12×12mm^2 cross-section were obtained with an accumulated area reduction of 85%. The as-rolled steel bars were then annealed for 3.6×10^{5}s at 723K. Samples for EBSD and TEM investigations were cut along the ND (the direction perpendicular to one of the edge of the square section) and RD of the rolled steel bars. The EBSD measurement was conducted on a Carl-Zeiss LEO-1550 Schottky FE-SEM, fitted with a TexSEM Lab. Orientation Imaging Microscope (OIM^{TM}) system with a spot size of approximately 30nm at 25kV. TEM observation was performed on a JEM-2000FXII microscope operated at 200kV.

To characterize the low-angle misorientations within the ferrite grains, the "misorientation kernel" approach was applied, in which the average misorientation of one point with all its six neighbors is calculated with the proviso that misorientations exceeding some tolerance value are excluded from the calculation. Since the EBSD scan step used in the present research was 0.1μm, the next-nearest neighbors were selected for defining the kernel. On the other hand, the Taylor factor was calculated using the subroutine involved in the OIM^{TM} system by inputting the texture results determined by EBSD, the strain gradient tensors and the slip systems, together with the CRSS for each slip system.

3. EXPERIMENTAL RESULTS

Figure 1 shows the microstructure in RD section in hot-rolled and warm-rolled conditions, respectively. Through grain area averaging the average grain size is determined to be 20 and 2.8μm in the two conditions, respectively. In the warm-rolled ultrafine-grained microstructure, there are two characteristic ferrite grains that show an area fraction peak, *i.e.* the fine ones (~1.5μm) and the coarse ones (~8μm). TEM confirmed that the polygonal ferrite grains of ~1μm in the RD section elongated along the rolling direction. The length to diameter ratio of the elongated grains is estimated to be 3~4. Meanwhile, grain boundaries are observed with either the imaging contrast between the neighboring

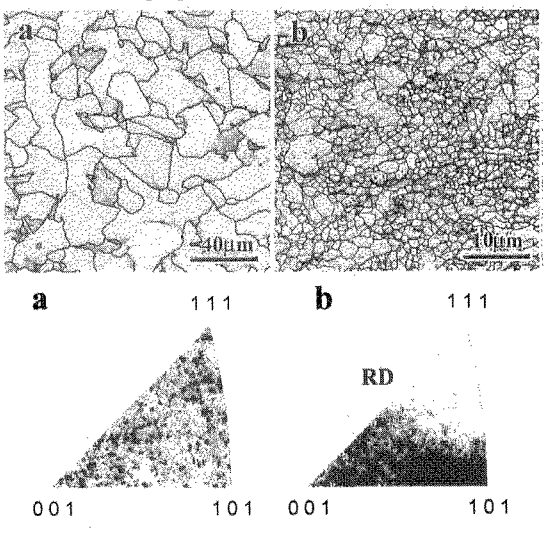

Figure 1. EBSD characterized microstructure in RD sections and the orientation distribution along RD of the low-carbon steel in hot-rolled (a) and warm-rolled (b) conditions, respectively.

grains or the borders that separate the regions with different substructures. The visibilities of the grain boundaries in the warm-rolled steel vary extensively in the TEM observation, and this can be attributed to the large fraction of low-angle boundaries revealed by the EBSD experiment. On the other hand, dislocation network or tangled cells are observed in most of the ferrite grains. Some grains are even quite clean with scarce dislocations. Larger cementite particles (~200nm) are usually found at grain boundaries, while the smaller ones (~20nm) tend to locate at the pile-ups of dislocations within the ferrite grains. The inverse pole figures (IPF) of the steel along RD are also shown in Fig. 1. In contrast tot the random ferrite orientation distribution of the hot-rolled steel, preferred ferrite orientations along the RD in the warm-rolled steel are clearly observed, *i.e.* mainly the <101> crystal directions spreading to the <001> and <113> directions. Meanwhile, the φ_2=45° section ODF of the ultrafine-grained microstructure indicated several concentrated orientations along the ND, such as {001}, {113}, {557} and {332}.

The preferred grain orientations in the warm-rolled steel can be sensitively reflected by the Taylor factor *M* at a certain deformation mode and slip system assumption. The ODF results indicate that caliber-rolling has produced the nearly random grain orientations in both ND and TD directions, and texture features is nearly only reflected on RD. In this case, the axisymmetric deformation along RD in the samples can be adequately assumed; therefore, the deformation gradient tensor, *F* is defined as:

$$F = \begin{bmatrix} 1 & 0 & 0 \\ 0 & -0.5 & 0 \\ 0 & 0 & -0.5 \end{bmatrix} \quad (3)$$

Meanwhile both the {110} <111> and {112} <111> slip systems are activated during the uniaxial tension deformation of ferrite grains. The critical resolved shear stress (CRSS) ratio ξ (where $\xi = CRSS_{\{hkl\}}/CRSS_{\{110\}}$) is supposed to be 1. As shown in Fig. 2a, the as-rolled steel shows the Taylor factor changing from 2.1 to 3.2. The average Taylor factor is then obtained to be 2.675 by averaging the detected orientations. The number fraction of the Taylor factor indicates the relative volume fraction of the ferrite grains that have the orientation corresponding to a certain Taylor factor. It is also found that the grains showing the higher Taylor factors are

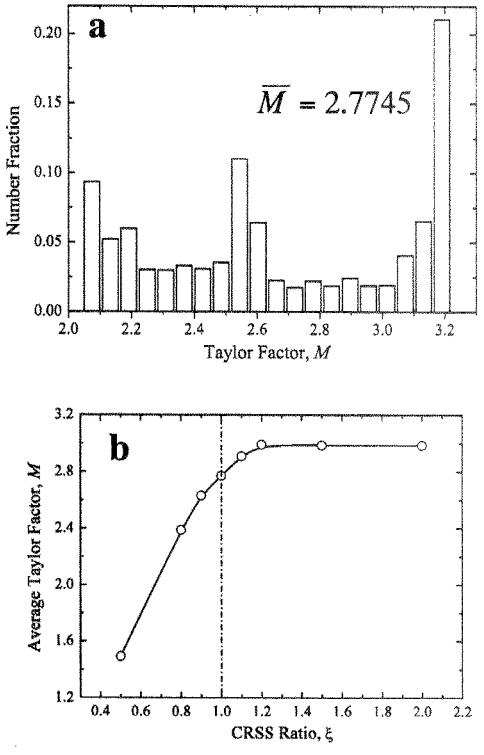

Figure 2. Taylor factor distribution of the warm-rolled steel under the uniaxial tension condition along RD (a), and the average Taylor factor depending on the CRSS ratio of 112 and 110 slip systems.

those oriented with RD//<101> or/and ND//{001}. Meanwhile the grains oriented to RD//{001} have the lower Taylor factors under the uniaxial tension deformation along the RD. Based on the EBSD orientation analysis of the warm-rolled steels, the average Taylor factors are plotted to the CRSS ratio and shown in Fig. 2b. The average Taylor factor clearly increases with the ratio in the range of 0.5-1.2 and reaches saturation when ratio becomes larger than 1.2. This shows that the microstructure with the concentrated orientation distribution exhibits a varying average Taylor factor that is quite sensitive to the CRSS ratio for different slip systems.

In contrast to the dislocation cells and cell boundaries that show no specific orientation in the deformed grains, dislocation cell-blocks tend to appear with the boundaries aligned to some specific crystal planes. Such specifically oriented boundaries within the deformed grains are constructed by a high-density of dislocations, and may increase the CRSS of the slip systems to different extents depending on the relative orientations between the boundaries and the slip planes [7]. Figure 3 shows the substructure of ferrite grains in the as-rolled ultrafine-grained steel. After the warm-rolling dislocation cells have not been observed as the characteristic substructural

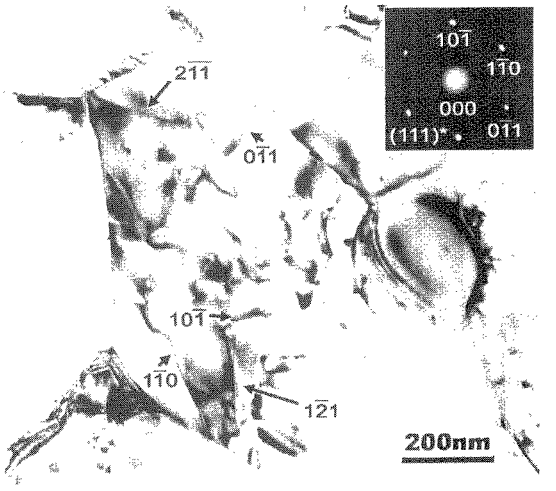

Figure 3. TEM micrographs on the ND section of the warm-rolled steel. Planar boundaries within the ferrite grains are observed parallel to {110} or {112} planes.

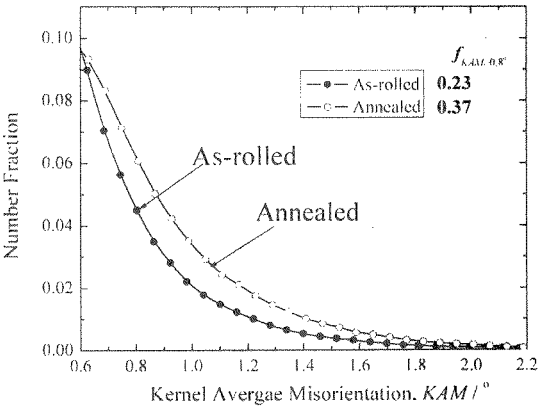

Figure 4. Kernel average misorientation (KAM) analysis of the image pixels in the 30×40μm OIM observed areas at the scanning step of 0.1μm.

feature in the deformed ferrite grains. Instead some linear contrasts were found in the grains. Since there is an obvious difference in the contrast between the two sides of the images, it is appropriate to consider those images as the low-angle boundaries. When the <111> direction of ferrite grain is tilted parallel to the incident electron beam, the boundaries show the sharp contrast. It seems that the boundaries are in the edge-on orientation to the {111} planes. Therefore, most of the boundaries can be indexed to be {110} or {112} planes. On the other hand, such line images with the thickened and elongated shapes have also been observed in the annealed sample. Annealing treatment at 723K seems to prompt the annihilation of randomly distributed dislocations, and simultaneously thickens the low-angle boundaries through the activated pile-up of dislocations on the existing boundaries.

Figure 4 shows the number fraction curves of kernel average misorientations (*KAM*) that are deduced from all the pixels in the 30×40 μm OIM images with a scanning

step of 0.1 μm. Excluding the pixels on grain boundaries defined by misorientations above 5°, the pixels in the grains show a distribution of *KAM* from 0 to 2.2°. The maximum fraction of pixels is observed at *KAM* = 0.6° in both the as-rolled and annealed samples. Since pixels with *KAM* >0.8° may produce the low-angle boundaries within the ferrite grains, the volume fraction of such boundaries with the grains can be obtained by accumulating the fractions of pixels with *KAM* >0.8°. It is shown that annealing increases the volume fraction of those low-angle boundaries extensively. Figure 5 shows the pixels with *KAM* >0.8° in a gray scale on the 10×24μm OIM images of grain boundaries (>5°), in the ND plane.

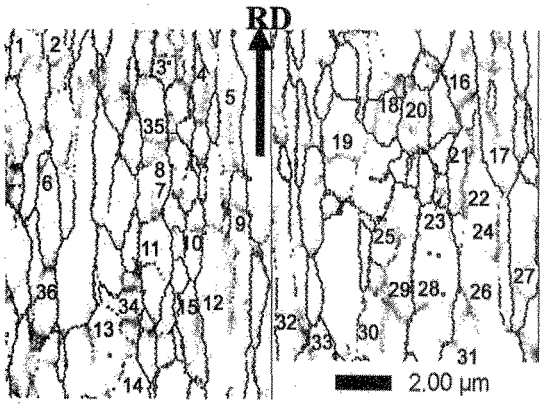

Figure 5. OIM micrographs showing the grain boundaries (? 5°) and the pixels with *KAM* >0.8° for the warm-rolled steel. 36 aligned pixel traces with *KAM*>0.8° in one measured area are numbered.

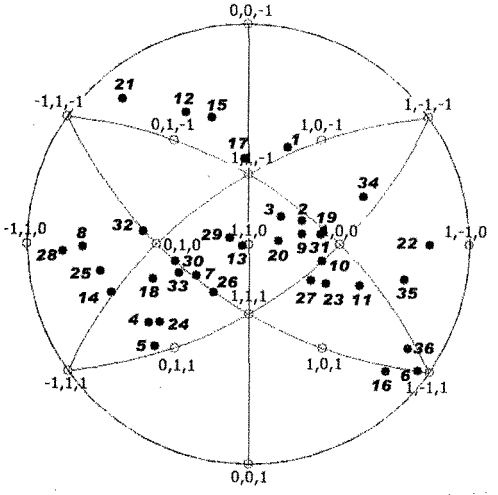

Figure 6. Crystallographic analysis results of the 36 aligned pixel traces with *KAM* >0.8° shown in Figure 5.

Most of the pixels with *KAM* > 0.8° constitute the aligned traces except for the few curved traces within the grains. Therefore, these aligned traces can be attributed to the planar boundaries described by the CBB model [5], and the curved traces to be caused by the dislocation cell boundaries.

To clarify the crystallographic feature of the traces, the crystal direction of the aligned traces are calculated with the orientations of the traces in each grain and the crystal orientation of that grain revealed by the OIM measurement. Figure 6 shows the crystal directions of the numbered aligned traces expressed in the [110] stereographic projection. The traces of {110} are shown in the projections to reflect the relative orientations of the boundary traces with *KAM* >0.8° with {110} planes. Meanwhile the angles between each crystal direction corresponding to one aligned trace and the 6 {110} and 12 {112} planes are calculated to find the most possible plane where the aligned traces may locate. It is found that only about half of the number aligned traces are observed to locate uniquely on one of the 18 crystal planes. Some of the traces locate on both {110} and {112} planes simultaneously, or belong to no one among the 18 choices. In the former case the multiple results for one aligned trace make it impossible to determine the corresponding plane orientation uniquely, and in the latter case the numbered align traces maybe the segments of dislocation cell boundaries that show no specific orientations. By counting the number of the aligned traces locating on {110} or {112} planes, the number Ratio of the Aligned Traces (R_{AT}) on the two crystal planes can be obtained. As a result, the ratio is 1.7 in the as-rolled state and decreases to 1.2 through the annealing treatment. The ratio is representative of the volume fraction ratio between the {110} type and {112} type cell-block boundaries (CBB), which influences the anisotropy of critical resolved shear stress (CRSS).

4. DISCUSSION

The substructural analysis of the as-rolled and annealed steel by the OIM method clarifies the volume fraction and the planar orientations of the low-angle boundaries (2° >*KAM* > 0.8°) within the ferrite grains. It is important to evaluate how those substructural features influence the CRSS of {110} and {112} slip systems and hence influence the average Taylor factor of the steel to explain the plastic deformation behavior of the steel. Peeters *et al.* proposed that dislocation cell-block boundaries (CBBs) that developed on the slip planes may induce the substructural anisotropy by changing the CRSS on {110} and {112} slip systems differently [5-7]. As shown in Eq. 2, τ_c^s depends on three factors, *i.e.* τ_0, the initial shearing resistance of the slip system, ρ^{CB}, cell boundary dislocations, and the contributions of CBBs. TEM observation has not clearly characterized the cell dislocation configuration in the as-rolled steel, and it seems reasonable to apply the average dislocation density into the second term of Eq. 2. In a previous work the average dislocation density of the same as-rolled and annealed steels was measured with the modified Warren-Averbach X-ray diffraction method [1]. The average dislocation density, ρ, was found to be 1.06 and $0.22\times10^{14}/m^2$ in the as-rolled and annealed steel. On the other hand, since nearly half of the OIM pixels with *KAM* > 0.8° are found to be of a planar character, the cell-block boundaries (CBBs) in the steels are tentatively considered to be half of the $f_{KAM>0.8^\circ}$ that is shown in Fig. 4. Meanwhile the dislocation density of the stable CBBs is supposed to be the same regardless of the deformation and annealing processes. Therefore, the dislocation density of the CBBs was predicted to be $1.3\times10^{15}/m^2$ [6].

$$\tau_{is}^{CBB} = \alpha G b \sqrt{\rho_i^{CBB}}\, abs(u_s^b \cdot u_i^{CBB})$$

The contribution of the CBBs to the CRSS of the slip systems is given by the following equation [9],

(4)

where α, G, b are the dislocation interaction parameter, the shear modulus and the magnitude of the Burgers vector, respectively. The symbol u_i^{CBB} denotes the unit vector that is perpendicular to the i family of planar CBBs and u_s^b the unit vector assigned to the slip direction of the system s. Then the average $abs(u_s^b \cdot u_i^{CBB})$ values of {110} and {112} CBBs, respective to the four <111> Burgers vectors can be calculated. To distinguish the additional increases in the CRSS of {110} and {112} slip systems that are caused by the two kinds of CBBs, we suppose tentatively that the {110} type CBBs mainly increase the CRSS of 112 slip systems and the {112} type CBBs increase that of the 110 slip systems. As a result Eq. 5 can be rewritten as the following equations:

$$\tau_{110}^{CBB} = \alpha G b \sqrt{\rho^{CBB}} \cdot abs(u_{110}^b \cdot u_{\{112\}}^{CBB}) \quad (5)$$

$$\tau_{112}^{CBB} = \alpha G b \sqrt{\rho^{CBB}} \cdot abs(u_{112}^b \cdot u_{\{110\}}^{CBB}) \quad (6)$$

When the constants, α, G, b and ρ^{CBB} are assigned the values of 0.2, 8.16×10^4 MPa, 2.48×10^{-10}m and 1.3×10^{15}m^{-2} [6], τ_{110}^{CBB} and τ_{112}^{CBB} are hence calculated to be 68.9 and 59.6 MPa, respectively. Meanwhile, the volume fraction (f) of the {110} and {112} CBBs can be obtained with the following equations:

$$f_{\{110\}}^{CBB} = \frac{1}{2} f_{KAM>0.8^o} \cdot \left(\frac{1}{1+R_{AT}}\right) \quad (7)$$

$$f_{\{112\}}^{CBB} = \frac{1}{2} f_{KAM>0.8^o} \cdot \left(\frac{R_{AT}}{1+R_{AT}}\right) \quad (8)$$

Where R_{AT} is the number ratio of the aligned traces on (112) and (110) planes. Therefore, in reference to Eq. 2, the CRSS of {110} and {112} slip systems is derived with the following equations:

$$\tau_{110}^c = \tau^0 + (1 - f_{\{110\}}^{CBB} - f_{\{112\}}^{CBB}) \cdot \alpha G b \cdot \sqrt{\rho} + f_{\{112\}}^{CBB} \cdot \tau_{110}^{CBB} \quad (9)$$

$$\tau_{112}^c = \tau^0 + (1 - f_{\{110\}}^{CBB} - f_{\{112\}}^{CBB}) \cdot \alpha G b \cdot \sqrt{\rho} + f_{\{110\}}^{CBB} \cdot \tau_{112}^{CBB} \quad (10)$$

With the present simplified model, the CRSS of {110} and {112} slip systems is calculated in the as-rolled and annealed conditions, respectively. We admit that the CBBs may influence the CRSS of the slip systems in more complex patterns and a more sophisticated equation should be constructed for that purpose.

The last parameter that needs to be determined is the initial shear resistance of the slip systems, *i.e.* τ^0. It is obvious that τ^0 should include all the hardening factors except for the dislocations in the microstructure. Pickering proposed an empirical equation for the estimation of yield strength of low-carbon steels [9]:

$$YS(MPa)=53.9+32.3[Mn\%]+83.2[Si\%]+17.4d^{-1/2} \quad (11)$$

where the content of Mn and Si is used in wt.% and the average grain size d is applied in mm. In this equation the constant, 53.9 is the value for the Peierls-Naborro stress, the solid solution hardening effect of C in ferrite. Applying the composition contents of Mn and Si and the average grain size of 3.1 μm to Eq. 11, the yield strength is derived to be 440.1MPa for the warm-rolled steel. Therefore, when $\overline{M} = 2.85$ is used for the randomly orientated ferrite grains under the uniaxial tension condition, τ^0 is then estimated by $YS/\overline{M}$ to be 154.4 MPa. However, the dispersion hardening of cementite particles in the warm-rolled microstructure should also be considered in addition to the solid solution hardening of Mn, Si and grain refinement hardening. The contribution of the cementite particles to the strength of ferrite is well described with the Ashby-Orowan relationship [10]:

$$\tau^{dispersion} = Gb/l \cdot \ln(r/b) \quad (12)$$

where r is the average radius of the particles, and l is the spacing between particles. The volume fraction of cementite within ferrite grains in the warm-rolled microstructure is about 1%, and the average diameter is observed to be 100nm. In consequence, the contribution of the cementite particles to the shearing resistance in the steel is estimated to be 20MPa [10]. Therefore τ^0 is finally determined to be 174.4MPa.

As shown in Table 1, the CRSS ratio of {112} to {110} slip systems is 0.99, approximately the same in both the as-rolled and annealed conditions. With the results of the average Taylor factor shown in Fig. 2, the average Taylor factor is thus derived to be 2.76 in both the as-rolled and annealed states. With the careful calculation the contribution of the CBBs to the CRSS of the slip systems is clarified in the warm-rolled and annealed ultrafine-grained steel. It is also found that the magnitudes of τ^{CBB} are quite smaller than those of τ_0 and τ^ρ. This result validates the assumption of equivalent CRSSs on {110} and {112} slip systems in the warm-rolled ultrafine-grained steels. In other words, the planar low-angle boundaries retained in the ferrite grains hardly cause the plastic anisotropy of warm-rolled steel by influencing the CRSS on different slip systems. Since the contributions of the planar low-angle boundaries to the yield strength of the warm-rolled steels are about 1~2%, the dislocation structure relevant contribution to yield strength of the warm-rolled or annealed steels can be adequately predicted with the changes in average dislocation density and the average Taylor factor, as well as the other microstructural features, such as grain refinement and cementite particle dispersion.

Compared to the normalized condition, the warm-rolling caused increase in yield strength of the steel

should be attributed to the following factors:

$$\Delta YS = \Delta YS^{solution} + \Delta YS^{refinement} + \overline{M} \cdot [\Delta\tau^{dispersion} + \Delta(\alpha \cdot Gb\sqrt{\rho})] \quad (13)$$

$\Delta YS^{solution}$ and $\Delta YS^{refinement}$ can be obtained feasibly by Pickering's empirical equation, i.e. Eq. 11. $\Delta\tau^{dispersion}$ can be obtained in Eq. 12. Therefore, it is possible to analyze the microstructural contributions to the yield strength of the warm-rolled steel. In the normalized condition, the yield strength can be decomposed into the contributions of solid solution hardening of Mn and Si, grain boundaries and dislocations. The contributions of the former two factors are calculated with Eq. 11, and the dislocation hardening effect can be estimated with a dislocation density of $5\times10^{11}m^{-2}$ for the annealed steels. There is a good agreement between the estimation and the experimental results in the normalized condition. In the warm-rolled condition, ferrite grains are refined, accompanying the elevated dislocation density and the dispersion of cementite particles in the as-rolled and annealed conditions. In the as-rolled and annealed steel, $\overline{M}$ =2.76 is used, and the YS contribution of grain refinement and cementite dispersion is calculated to be 312.5 and 55.2MPa, respectively. When the average dislocation density and dislocation interaction parameter α=0.2 are applied, the dislocation contribution is 115 and 52.4MPa in the as-rolled and annealed conditions, respectively. Comparing the sum of the contributions with the experimental results, only about a 20MPa overestimation of yield strength is observed. Meanwhile, the decrease of yield strength caused after annealing can be well described with the decrease of dislocation density, which means that α=0.2 is appropriate for the warm-rolled dislocation structure in the steel.

Table 1. The parameters applied and calculation results of the contributions to the CRSS of 110 slip system and 112 slip systems using Eq. 4~10, for the steel in as-rolled and annealed conditions, respectively.

	ρ $10^{14}m^{-2}$	$f^{CBB}_{\{110\}}$	$f^{CBB}_{\{112\}}$	f^{dis}	τ^{ρ}	τ^{CBB}_{110}	τ^{CBB}_{112}	τ^{c}_{110}	τ^{c}_{112}	ξ
As-rolled	1.06	0.043	0.074	0.885	36.88	5.0	2.5	216.3	213.8	0.988
Annealed	0.22	0.084	0.10	0.815	15.47	6.9	5.0	196.8	194.9	0.990

CONCLUSIONS

The texture and substructural features in warm-rolled ultrafine-grained low-carbon steel were examined with the orientation imaging microscopy and TEM observation. Column-shaped ferrite grains elongated along the RD were observed in the ultrafine-grained steel. The average grain size was refined to about 3μm with the warm-rolling. <110>//RD fiber texture was clearly revealed. A lower average Taylor factor was predicted in the fiber texture developed ultrafine-grained microstructure, while assuming the same critical resolved shear stress (CRSS) on {110} and {112} slip system. It was found that the average Taylor factor was sensitive to the CRSS ratio between the two slip systems.

TEM observation confirmed the existence of both {110} and {112} type cell-block boundaries (CBB) in the caliber-rolled low-carbon steels, besides the randomly distributed dislocations. The number fraction and orientations of those CBBs were characterized by OIM analysis with the kernel average misorientation (*KAM*) calculation. The traces of the low-angle boundaries with *KAM* >0.8° were observed to be almost completely aligned. Annealing treatment increased the volume fraction of the low-angle boundaries from 0.23 to 0.37. Crystallographic orientation determination of those aligned traces by OIM analysis showed that half of those low-angle boundaries were planar boundaries distinctively parallel to {110} or {112} planes. The number ratio of the planar boundaries parallel to {110} and {112} planes was deduced and found to be different between the as-rolled and annealed conditions. Using the model proposed by Peeters *et. al*, the CRSS of {110} and {112} slip systems involving the contributions of both the randomly distributed dislocations and the CBBs were calculated. The CBBs were found to occupy less than 2% of the total CRSS of the slip systems. The influence on the average Taylor factor of the CRSS ratio on {112} and {110} slip systems could be reasonably ignored. The microstructural contributions to the macroscopic yield strength in normalized, warm-rolled and annealed conditions were estimated involving the hardening effects of solid solution, grain refinement, cementite dispersion, as well as the average Taylor factor and dislocation density. A good agreement was obtained between the estimation and experimental results.

REFERENCES

[1] F. Yin, T. Hanamura, O. Umezawa and K. Nagai: Mater. Sci. Eng., A354, 31-39(2003).
[2] U. F. Kocks: Metall. Trans., l.1, 1121-43(1970).
[3] A. B. Lopes, E. F. Rauch and J. J. Gracio: Acta Metall. Mater., 47, 859-66(1999).
[4] B. Orlans-joliet, J. H. Driver and F. Montheiliet: Acta Metall. Mater., 38, 581-94(1990).
[5] B. Peeters, M. Seefeldt, P. Van Houtte and E. Aernoudt: Scripta Mater., 45, 1349-56(2001).
[6] B. Peeters, M. Seefeldt, C. Teodosiu, S.R. Kalidindi, P. Van Houtte and E. Aernoudt: Acta Metall. Mater., 49, 1607-19(2001).
[7] B. Peeters, B. Bacroix, C. Teodosiu, P. Van Houtte and E. Aernoudt: Acta Metall. Mater., 49, 1621-32(2001).
[8] X. Huang and D. J. Jenson: Electron Backscattering Diffraction in Material Science, Ed. A.J. Schwartz, M. Kumar, and B.L. Adams, Kluwer Academic/Plenum Publishers, London (2000) pp.265-276.
[9] K. Nagai: J. Mater. Proc. Techno., 5187, 1-4(2001).
[10] M. F. Ashby: Acta Metall., 14, 679-85(1966).

(Received December 1, 2003; Accepted July 20, 2004)